

Coherent noise cancellation in optomechanical system with double optical modes

Jiashun Yan¹ and Jun Jing^{1,*}

¹*Zhejiang Province Key Laboratory of Quantum Technology and Device,
Department of Physics, Zhejiang University, Hangzhou 310027, Zhejiang, China*

A quantum metrology protocol for continuous force sensing is developed beyond the quantum standard limit on performing a coherent quantum noise cancellation (CQNC) strategy in an optomechanical system, that consists of two optical modes with non-identical frequencies and a mechanical mode. In particular, an ultrasensitive susceptibility around the mechanical-mode frequency is solely achieved with driving the higher-frequency optical mode and probing the lower-frequency one. More importantly, this asymmetrical and unique treatment allows the ancillary optical mode to constitute an effective coherent channel for implementing the CQNC strategy, when the ancillary mode is set to be near-resonant with the probe mode to avoid the disturbance from the driven mode. The ancillary mode then acts as a negative-frequency mechanical oscillator to offset the backaction noise arising from both radiation-pressure and driving. Under the condition of strong driving and strong coupling, the measurement sensitivity as well as the signal-to-noise ratio in our optomechanical-sensing scheme is therefore found to be significantly enhanced by about two orders in magnitude, comparing to that without noise cancellation. In addition, our scheme can be practiced in a tripartite optomechanical setup with a membrane in the middle and a twisted-cavity-based weak-torque detector.

I. INTRODUCTION

At the intersection of nanophysics and quantum optics, quantum optomechanics explores the interactions between the electro-magnetic radiation and the mechanical-oscillator motion. In the Fabry-Perot cavity typically used in the cavity optomechanics, the light field exerts a radiation pressure on a vibrating mirror [1]. Myriad applications on the radiation pressure have been realized by the cavity optomechanics, such as cooling the motion of oscillators to their ground states [2–6], demonstrating the quantum-to-classical transitions [7], and controlling the photon transport [8]. Among these quantum science and technologies, the ultrasensitive measurement or detection about the weak force on the mechanical oscillator are under intensive investigations [9–12] as a significant branch of quantum metrology [13, 14].

Optomechanical systems are also well known for providing an efficient way of converting the quantum information at MHz frequencies (mechanical motion) up to optical frequencies [15]. They have to be subject to hybrid noises from various sources or environmental degrees of freedom. The noises induce errors to sensing or measurement with the mechanical motion, because they cannot be distinguished from the signal and always undetermined to observers. The weak-force sensing by optomechanical systems then desires simultaneously a high susceptibility to magnify the external force and an effective suppression over the measurement noise, as the noise might be synchronously amplified. The measurement noise generally consists of the shot noise and the backaction noise [16–18]. The shot noise is induced by photon number-phase uncertainty limiting the high-precision in-

terferometric experiments, such as the laser interferometer gravitational-wave observatory [19], which decreases with the pumping power. While the backaction noise results from the fluctuations in the radiation-pressure of the cavity optical mode, which increases with the pumping power and was observed for the first time in Refs. [20, 21]. Then the trade-off between these two noises leads to a lower bound for the detection sensitivity, i.e., the standard quantum limit (SQL) [16].

Various methods for the optomechanical force-sensor to break through SQL have been proposed to offset the backaction noise, such as the frequency-dependent squeezing of the input light [22–25], the variational measurement [25–27], and the application of the dual mechanical resonators [28, 29] or an optical spring [30, 31] to modify the mechanical response function. Compared to these backaction-evading techniques, a pure quantum protocol named coherent quantum noise cancellation (CQNC) recently suggested by Tsang and Caves [32] could interfere destructively with the backaction noise at all frequencies by the antinoise process of an deliberately designed ancillary mode. In this work, the CQNC strategy as a judicious protocol to remove measurement noise is developed from a single-optical-mode optomechanical system [33] to a double-optical-mode one. The multi-mode optomechanical systems [34–36] claim to have a higher sensitivity by the generated squeezed states due to the interaction between the cavity photons and the mechanical oscillator [37] than the single-mode system. While with respect to the CQNC scheme, the multi-mode system might import additional measurement noises raised by the detuning between the system modes and the ancillary mode. In a double-optical-mode system, driving the high-frequency optical mode and detecting the low-frequency one are found to be crucial and nontrivial prerequisites to realize the CQNC. The two-mode system can then be reduced to an effective single-

* Email address: jingjun@zju.edu.cn

mode one and the driven-mode fluctuation becomes separable in the whole dynamics after the linearization process. It is shown that our protocol avoids the normal-mode splitting induced by the strong coupling between the optical modes and the mechanical mode to obtain the high sensitivity around the mechanical-mode frequency. In addition, when the ancillary optical mode is tuned to be near-resonant with the probe mode, the desired noise cancellation is followed by building an effective coherent channel to compensate the backaction noise. Our scheme can be performed in both a conventional “membrane-in-the-middle” setup [37–40] and a novel twisting optomechanical cavity consisting of a torsional mechanical oscillator [41].

The rest of this work is structured as following. In Sec. II, the Hamiltonian is analysed for our optomechanical system with two optical modes of non-identical frequencies. Strong coupling between the optical modes and the mechanical mode is required for the CQNC strategy, which depends on a sufficiently large pumping power. The Routh-Hurwitz criterion, however, places a limit on the pumping power according to the system stability. Respecting this limit, we proceed to linearize the relevant quantum Heisenberg-Langevin equations. In Sec. III, the susceptibility of the mechanical oscillator and the standard quantum limit are calculated to evaluate the sensing performance of the system. Then the normal mode splitting is discussed as a hallmark of the strong coupling. In Sec. IV, the microscopic mechanism of the measurement-noise cancellation is illustrated under the CQNC protocol for the double-optical-mode optomechanical system. An improved sensitivity for the weak-force metrology and the relevant signal-to-noise ratio (SNR) are demonstrated to break through the SQL under the system-stability condition. In Sec. V, two optomechanical setups are presented to realize the system Hamiltonian in our model available for control. We summarize the whole work in Sec. VI.

II. MODEL AND HAMILTONIAN

We start with a general optomechanical system consisting of two optical modes with different frequencies and a mechanical mode. With one of the optical modes under driving, the system Hamiltonian can be written as ($\hbar \equiv 1$)

$$H = \omega_a a^\dagger a + \omega_b b^\dagger b + \frac{\omega_m}{2} (x^2 + p^2) + gx(a^\dagger b + ab^\dagger) + iE(a^\dagger e^{-i\omega_L t} - ae^{i\omega_L t}), \quad (1)$$

where a, b (a^\dagger, b^\dagger) are respectively the annihilation (creation) operators of the high-frequency and the low-frequency optical modes, and ω_a and ω_b are their frequencies, $\omega_a > \omega_b$. $x \equiv x_m/x_{\text{ZPF}}$ and $p \equiv p_m x_{\text{ZPF}}$ are respectively the dimensionless position and momentum operators of the mechanical oscillator, where $x_{\text{ZPF}} \equiv 1/\sqrt{m\omega_m}$ is the zero point fluctuation with ω_m the frequency and m the mechanical-oscillator mass. g is the coupling strength

between the optical modes and the mechanical mode and this nonlinear optomechanical interaction can be realized by the double-side radiation-pressure or the permittivity tensor modulation (The details are left to Sec. V). $E \equiv \sqrt{P_{\text{in}}\kappa_a/\omega_L}$ is the driving strength determined by the driving power P_{in} , the cavity damping coefficient κ_a and the driving-laser frequency ω_L .

The mechanical oscillator is supposed to couple to a Markovian environment through the damping loss. Then in the rotating frame with respect to $H_L = \omega_L(a^\dagger a + b^\dagger b)$, the following Heisenberg-Langevin equations are obtained through the input-output theory:

$$\begin{aligned} \dot{a} &= -i\Delta_a a - igxb - \kappa_a a + \sqrt{2\kappa_a}a_{\text{in}} + E, \\ \dot{b} &= -i\Delta_b b - igxa - \kappa_b b + \sqrt{2\kappa_b}b_{\text{in}}, \\ \dot{x} &= \omega_m p, \\ \dot{p} &= -\omega_m x - g(a^\dagger b + ab^\dagger) - \gamma_m p + F_{\text{in}}. \end{aligned} \quad (2)$$

Here $\Delta_{a,b} \equiv \omega_{a,b} - \omega_L$ is the detuning between the optical mode a (b) and the driving laser. κ_i ($i = a, b$) and γ_m are respectively the relaxation rates of the optical and mechanical modes. a_{in} and b_{in} account for the noise operators associated with the individual input fields. Due to the fluctuation-dissipation theorem, the autocorrelation functions of the vacuum noises for the optical modes satisfy $\langle a_{\text{in}}(t)a_{\text{in}}^\dagger(\tau) \rangle = \langle b_{\text{in}}(t)b_{\text{in}}^\dagger(\tau) \rangle = \delta(t - \tau)$. F_{in} consists of the to-be-determined external force F_{ext} acting on the oscillator and the input noise of the oscillator ξ satisfying $\langle \xi(t)\xi(\tau) \rangle \approx 2\gamma_m n_{\text{th}}\delta(t - \tau)$, where $n_{\text{th}} \equiv 1/(e^{\omega_m/T} - 1)$ denotes the average population of the mechanical oscillator ($k_B \equiv 1$).

The linearization process by decomposing the operators into the expectation-value part (time-independent) and the fluctuating part (time-dependent) is valid under a sufficiently large amplification coefficient by a strong pumping or driving. Under this condition, one can write $O = \langle O \rangle + \delta O$, where O is an arbitrary operator and $\langle O \rangle$ is the expectation value with respect to the steady-state of the system. Inserting the decomposed expressions into Eq. (2), one can find that $\langle a \rangle = \alpha = E/(i\Delta_a + \kappa_a)$, $\langle b \rangle = 0$, $\langle x \rangle = 0$, and $\langle p \rangle = 0$. Omitting the quadratic terms $\delta x\delta b$, $\delta x\delta a$, $\delta a^\dagger\delta b$, and $\delta a\delta b^\dagger$, and reexpressing the fluctuation variables $\delta O \rightarrow O$, one can have the linearized quantum Heisenberg-Langevin equations as following (up to a phase modulation over the operator b):

$$\begin{aligned} \dot{a} &= -i\Delta_a a - \kappa_a a + \sqrt{2\kappa_a}a_{\text{in}}, \\ \dot{b} &= -i\Delta_b b - iGx - \kappa_b b + \sqrt{2\kappa_b}b_{\text{in}}, \\ \dot{x} &= \omega_m p, \\ \dot{p} &= -\omega_m x - G(b^\dagger + b) - \gamma_m p + F_{\text{in}}, \end{aligned} \quad (3)$$

where $G \equiv |\alpha|g$. Note now the dynamics and the noise field of the driven mode- a are decoupled from that of optical mode- b and the mechanical oscillator. Nevertheless the coefficient $|\alpha|$ indicates a significant amplification on the effective coupling between the probe mode and the mechanical mode.

It is interesting to make an argument here about the choice of the driving mode and the probe mode in the initial Hamiltonian (1) before further discussion. First, the choice of simultaneously driving both optical modes has been ruled out. In that scenario, the expectation value $\langle b \rangle$ will be nonvanishing, so that after the linearization process the mode a can *not* be decoupled from the whole dynamics hindering the following metrology. Second, if one drives the low-frequency optical mode- b and probes the high-frequency one, i.e., modifies the driving term in Eq. (1) by $a \rightarrow b$, then through a similar derivation one can arrive at

$$\begin{aligned}\dot{b} &= -i\Delta_b b - \kappa_b b + \sqrt{2\kappa_b} b_{\text{in}}, \\ \dot{a} &= -i\Delta_a a - iG' x - \kappa_a a + \sqrt{2\kappa_a} a_{\text{in}}, \\ \dot{x} &= \omega_m p, \\ \dot{p} &= -\omega_m x - G'(a^\dagger + a) - \gamma_m p + F_{\text{in}},\end{aligned}\quad (4)$$

where $G' = |\langle b \rangle|g$. An intuitive insight tells no obvious difference between Eq. (3) and Eq. (4). Both of them describe an effective single-mode optomechanical system. However, to solely drive one of these two modes with different frequencies, ω_L has to be near-resonant with ω_a to attain Eq. (3) or be near-resonant with ω_b to attain Eq. (4). Then the coefficients $\Delta_b < 0$ in Eq. (3) and $\Delta_a > 0$ in Eq. (4), correspond respectively to the blue-detuning and the red-detuning cases in practice. The linearized Heisenberg-Langevin equations (3) and (4) are therefore *not* symmetrical to each other, even upon $a \leftrightarrow b$. These two imbalanced sidebands will manifest dramatically different results for the weak-force detection in terms of the system stability, the normal-mode splitting and the CQNC strategy (The detailed analysis can be found in the following sections). In short, we find that driving the high-frequency mode and probing the low-frequency mode are available to break through the SQL in quantum metrology over the mechanical mode. This nontrivial choice justifies our Hamiltonian in Eq. (1) as well as the dynamics by Eq. (3) in this specific optomechanical system with double optical modes.

From Eq. (3), a large coupling-strength G determined by the initial coupling-strength g and the average photon number in the cavity $|\alpha|^2$ is demanded to realize the CQNC strategy [33]. It is found that the Routh-Hurwitz stability criterion, however, restricts the value of $|\alpha|$. In particular, the real part of all the roots of the system characteristic polynomial must be negative [42] to ensure the stability of the linear system. For our optomechanical system, the Routh-Hurwitz criterion yields

$$|\alpha|^2 > -\frac{(\Delta_b^2 + \kappa_b^2)\omega_m}{2|\Delta_b|g^2}, \quad (5)$$

under the blue-detuning situation $\Delta_b < 0$ and

$$|\alpha|^2 < \frac{(\Delta_b^2 + \kappa_b^2)\omega_m}{2|\Delta_b|g^2}, \quad (6)$$

under the red-detuning situation $\Delta_b > 0$ [make $a \rightarrow b$ in Eq. (4)], respectively. The detailed calculation can be

found in appendix A. Thus it is clear that the average photon number $|\alpha|^2$ determined by the driving power is under a magnitude restriction when one drives the low-frequency optical mode while probing the high-frequency one, i.e., in the red-detuning case $\Delta_b > 0$. In contrast, the system stability can be always satisfied in the blue-detuning case $\Delta_b < 0$, since Eq. (5) always holds. To be specific in practice, when $\Delta_b = \omega_m$, the restriction in Eq. (6) yields that $G^2 < (\omega_m^2 + \kappa_b^2)/2 \approx \omega_m^2/2$. The system evolution will then become unstable when the coupling strength becomes comparable to the mechanical frequency. While with the blue-sideband driving $\Delta_b = -\omega_m$, the stable condition $G^2 > -(\omega_m^2 + \kappa_b^2)/2$ holds all the time.

III. WEAK FORCE DETECTION WITHOUT CQNC

A. Mechanical susceptibility and standard quantum limit

For quantum metrology, the mechanical motion is not usually analyzed in the time domain. In practice, it is convenient to transform the time evolution of system into the frequency domain to analyse the linear response in the noise spectrum of the mechanical oscillation to the external force [1]. By the Fourier transformation $O(\omega) \equiv \frac{1}{2\pi} \int dt O(t) e^{i\omega t}$ for all the operators, the dynamics of the system (leave out the driven mode- a) in Eq. (3) can then be displayed in the frequency space:

$$\begin{aligned}-i\omega x &= \omega_m p, \\ (\gamma_m - i\omega)p &= -\omega_m x - \sqrt{2}Gx_b + F_{\text{in}}, \\ (\kappa_b - i\omega)x_b &= -\kappa_b x_b + \Delta_b p_b + \sqrt{2\kappa_b}x_{\text{in}}^b, \\ (\kappa_b - i\omega)p_b &= -\Delta_b x_b - \sqrt{2}Gx + \sqrt{2\kappa_b}p_{\text{in}}^b,\end{aligned}\quad (7)$$

where the quadratures are $x_b \equiv (b + b^\dagger)/\sqrt{2}$, $p_b \equiv (b - b^\dagger)/\sqrt{2}i$ and the relevant noise operators are $x_{\text{in}}^b \equiv (b_{\text{in}} + b_{\text{in}}^\dagger)/\sqrt{2}$, $p_{\text{in}}^b \equiv (b_{\text{in}} - b_{\text{in}}^\dagger)/\sqrt{2}i$. Solving the linear equations (7), one could find $x(\omega)$ as a function of variables F_{in} , x_{in}^b and p_{in}^b :

$$x(\omega) = \chi(\omega) \left\{ F_{\text{in}}(\omega) - \frac{2\sqrt{\kappa_b}G}{(\kappa_b - i\omega)^2 + \Delta_b^2} \right. \\ \left. \times [(\kappa_b - i\omega)x_{\text{in}}^b(\omega) + \Delta_b p_{\text{in}}^b(\omega)] \right\}, \quad (8)$$

where $\chi(\omega)$ is defined as the susceptibility of the mechanical oscillation:

$$\chi(\omega) = \left[\frac{\omega_m^2 - i\omega\gamma_m - \omega^2}{\omega_m} - \frac{2G^2\Delta_b}{(\kappa_b - i\omega)^2 + \Delta_b^2} \right]^{-1}. \quad (9)$$

In the linear-response function described in Eq. (8), the optomechanical system can be viewed as a linear amplifier for the input fields individually from the optical

mode b and the mechanical oscillator. The real and imaginary parts of the susceptibility in Eq. (9) imply respectively the dissipation rate (proportional to G^2) and the mechanical-frequency shift due to the inner-couplings of the optomechanical system.

The phase shift of the transmitted or the reflected light of the optical-mode b allows an indirect measurement for the displacement of the mechanical-oscillator under the external force. The measurement often requires a homodyne detector, in which the signal is brought into interfere with a local oscillator as a phase reference. Based on the input-output theory, we have

$$\begin{aligned} x_{\text{out}}^b(\omega) &= \sqrt{2\kappa_b}x_b(\omega) - x_{\text{in}}^b(\omega), \\ p_{\text{out}}^b(\omega) &= \sqrt{2\kappa_b}p_b(\omega) - p_{\text{in}}^b(\omega). \end{aligned} \quad (10)$$

The output field will carry information about the inner field, then the force acting on the mechanical oscillator could be estimated by the continuous homodyne measurement of the quadratures of the output signal

$$\begin{aligned} M(\omega) &= \sin\varphi x_{\text{out}}^b(\omega) + \cos\varphi p_{\text{out}}^b(\omega) \\ &= \chi_F(\omega)F_{\text{in}}(\omega) + \chi_x(\omega)x_{\text{in}}^b(\omega) + \chi_p(\omega)p_{\text{in}}^b(\omega), \end{aligned} \quad (11)$$

where

$$\chi_F(\omega) = \frac{-2\sqrt{\kappa_b}G[\Delta_b \sin\varphi + (\kappa_b - i\omega) \cos\varphi]}{(\kappa_b - i\omega)^2 + \Delta_b^2} \chi(\omega), \quad (12)$$

$$\begin{aligned} \chi_x(\omega) &= \frac{(\kappa_b^2 + \omega^2 - \Delta_b^2) \sin\varphi - 2\kappa_b\Delta_b \cos\varphi}{(\kappa_b - i\omega)^2 + \Delta_b^2} \\ &+ \frac{4\kappa_bG^2(\kappa_b - i\omega)[\Delta_b \sin\varphi + (\kappa_b - i\omega) \cos\varphi]}{[(\kappa_b - i\omega)^2 + \Delta_b^2]^2} \chi(\omega), \end{aligned} \quad (13)$$

$$\begin{aligned} \chi_p(\omega) &= \frac{(\kappa_b^2 + \omega^2 - \Delta_b^2) \cos\varphi + 2\kappa_b\Delta_b \sin\varphi}{(\kappa_b - i\omega)^2 + \Delta_b^2} \\ &+ \frac{4\kappa_bG^2\Delta_b[\Delta_b \sin\varphi + (\kappa_b - i\omega) \cos\varphi]}{[(\kappa_b - i\omega)^2 + \Delta_b^2]^2} \chi(\omega). \end{aligned} \quad (14)$$

Here φ is the phase of the local oscillator (LO) field and could be modulated by an electro-optical modulator [43]. For simplicity, φ is set as zero in following discussion. So that we only need measure the phase quadrature by homodyne detection. $\chi_F(\omega)$ characterizes the amplification of the detection signal. $\chi_x(\omega)$ and $\chi_p(\omega)$ are regarded as the noisy signals in comparison to $\chi_F(\omega)$. To analyse the spectral density of these measurement noises, one can define an effective force noise:

$$\begin{aligned} F_N(\omega) &\equiv \frac{M(\omega)}{\chi_F(\omega)} - F_{\text{ext}}(\omega) \\ &= \xi(\omega) + \frac{\chi_x(\omega)}{\chi_F(\omega)}x_{\text{in}}^b(\omega) + \frac{\chi_p(\omega)}{\chi_F(\omega)}p_{\text{in}}^b(\omega). \end{aligned} \quad (15)$$

Then the quantum noise spectrum $S(\omega)$ can be obtained

by [44]

$$S(\omega) = \frac{1}{2}[S_{FF}(\omega) + S_{FF}(-\omega)], \quad (16a)$$

$$S_{FF}(\omega) = \int d\omega' \langle F_N(\omega)F_N(\omega') \rangle, \quad (16b)$$

in which the thermal-noise spectrum is expressed by

$$S_{\text{th}}(\omega) = \int d\omega' \langle \xi(\omega)\xi(\omega') \rangle \approx 2\gamma_m n_{\text{th}}. \quad (17)$$

And due to the fact that the vacuum input noise $b_{\text{in}}(t)$ satisfies the δ -correlation function, the noise spectrum without control is then expressed as

$$\begin{aligned} S(\omega) &= S_{\text{th}}(\omega) + \frac{\Delta_b(\Delta_b^2 - \omega^2 + 3\kappa_b^2)\Delta}{2\kappa_b\omega_m(\omega^2 + \kappa_b^2)} + \frac{G^2(\Delta_b^2 + 4\kappa_b^2)}{2\kappa_b(\omega^2 + \kappa_b^2)} \\ &+ \frac{[(\Delta_b^2 - \omega^2 + \kappa_b^2)^2 + 4\kappa_b^2\omega^2](\omega^2\gamma_m^2 + \Delta^2)}{8G^2\kappa_b\omega_m^2(\omega^2 + \kappa_b^2)}, \end{aligned} \quad (18)$$

where $\Delta \equiv \omega^2 - \omega_m^2$. The second term on the right-hand side of Eq. (18) takes the role of the background noise (independent of the coupling-strength G) induced by the detuning between the measured frequency and the mechanical-oscillator frequency. The third term scaling as G^2 denotes the backaction noise. The last term scaling as $1/G^2$ is called the shot noise or the imprecision noise [16, 17]. The lower bound of the noise spectrum with the optimized value of G in Eq. (18)

$$G_L = \left\{ \frac{[(\Delta_b^2 - \omega^2 + \kappa_b^2)^2 + 4\kappa_b^2\omega^2](\omega^2\gamma_m^2 + \Delta^2)}{4\Delta_b^2\omega_m^2 + 16\kappa_b^2\omega_m^2} \right\}^{\frac{1}{4}} \quad (19)$$

is the standard quantum limit for continuous force sensing [45]:

$$\begin{aligned} S_L(\omega) &= S_{\text{th}} + \frac{1}{2\kappa_b\omega_m(\omega^2 + \kappa_b^2)} [\Delta_b(\Delta_b^2 - \omega^2 + 3\kappa_b^2)\Delta + \\ &\sqrt{(\Delta_b^2 + 4\kappa_b^2)(\omega^2\gamma_m^2 + \Delta^2)} \sqrt{(\Delta_b^2 - \omega^2 + \kappa_b^2)^2 + 4\kappa_b^2\omega^2}]. \end{aligned} \quad (20)$$

It places a limit on the detector sensitivity about the weak signal, which can be certainly broken though via a quantum-control strategy, such as the coherent quantum noise cancellation.

B. Strong coupling and Normal-mode splitting

The strong coupling between the probe mode and the mechanical mode is a prerequisite for the coherent quantum noise cancellation strategy. It is usually marked by the phenomenon of the normal mode splitting (NMS) or the avoided NMS. In general, NMS occurs in a coupled two-partite system with an energy-exchange interaction larger than the decoherence rate of the system [46]. This section is contributed to analysing the detection sensitivity through the NMS phenomena under the red-sideband

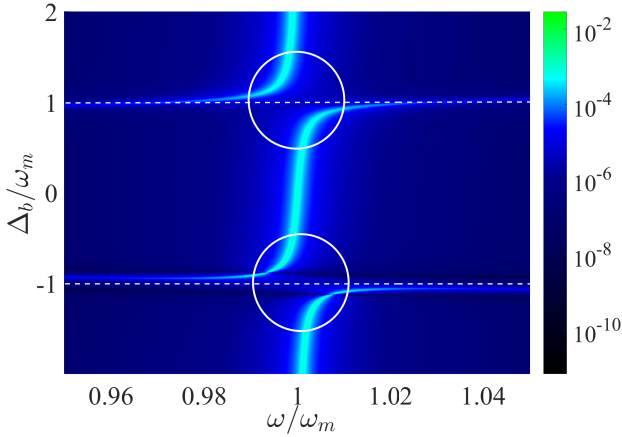


FIG. 1. (Color online) The absolute value of the imaginary part of the mechanical susceptibility $|\text{Im}\chi(\omega)|$ as a function of the normalized frequency ω/ω_m and the detuning Δ_b/ω_m . The other parameters are set as $\kappa_b = 10^{-2}\omega_m$, $G = 4\kappa_b$ and $\gamma_m = 1.2 \times 10^{-3}\omega_m$.

$\Delta_b = \omega_m$ and the blue-sideband $\Delta_b = -\omega_m$ situations. As emphasised in Sec. II, these two particular sidebands correspond to the case of driving the low-frequency optical mode and probing the high-frequency optical mode and the opposite case, respectively.

In Fig. 1, the absolute value of the imaginary part of the mechanical-mode susceptibility $|\text{Im}\chi(\omega)|$ is plotted as a function of normalized frequency ω/ω_m and normalized detuning Δ_b/ω . $\text{Im}\chi(\omega)$ is regarded as the effective dissipation rate for the mechanical oscillator and used to identify the NMS phenomena [15] in the parametric space. Under the condition $G = 4\kappa_b$, each sideband exhibits a clear bifurcation demonstrating that the mode splitting and the detection sensitivity will obtain extreme values around these bifurcations. Note if the effective coupling strength is less than the optical dissipation rate $G < \kappa_b$, then the splitting around the two sidebands would not occur any more.

The NMS phenomenon can be deliberately observed through the noise spectrum and the susceptibility with various coupling strengths. In the red-sideband situation [see Fig. 2(a)(c)], both the noise spectrum and the susceptibility are splitted into a double-valley or a double-peak pattern symmetrical to the mechanical-oscillator frequency when $G > \kappa_b$, where the peak or valley separation becomes even larger with a stronger coupling. In contrast, the avoided NMS pattern illustrated in Fig. 1 is clearly observed in the blue-sideband situation [e.g., Fig. 2(b)(d)]. The susceptibility displays a single-valley or a single-weak pattern around ω_m , featuring a larger amplification in magnitude around the near-resonant regime for ω_m under a stronger coupling strength.

Both NMS and avoided NMS phenomenon can be understood by the linearized Heisenberg-Langevin equations (3) describing the fluctuation dynamics around the

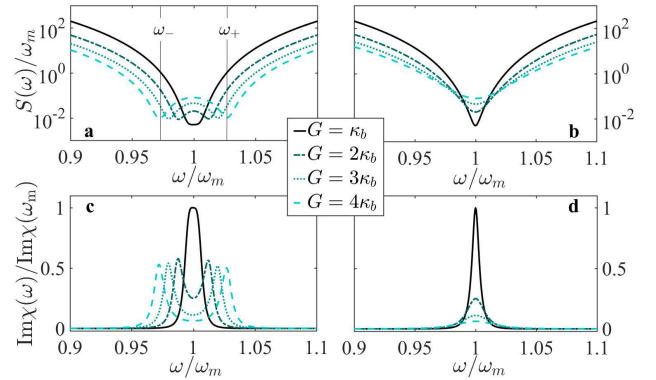


FIG. 2. (Color online) The normalized noise spectrum $S(\omega)/\omega_m$ as a function of the normalized frequency ω/ω_m with various coupling strength G for the red-sideband $\Delta_b = \omega_m$ (a) and the blue-sideband $\Delta_b = -\omega_m$ situation (b), respectively. The ratio of the imaginary parts of the mechanical susceptibilities $\text{Im}\chi(\omega)/\text{Im}\chi(\omega_m)$ as a function of ω/ω_m for the red-sideband (c) and the blue-sideband situation (d), respectively. Note here $\chi(\omega_m)$ is the susceptibility with a fixed coupling strength $G = \kappa_b$ for the mechanical frequency ω_m . The dissipation rates of the probe mode and the mechanical mode are respectively $\kappa_b = 10^{-2}\omega_m$ and $\gamma_m = 1.2 \times 10^{-3}\omega_m$. The average population for the thermal noise is set as $n_{\text{th}} = 10$ [44].

steady states of both the mechanical mode and the probe mode. The equation (3) can be alternatively obtained by the effective Hamiltonian:

$$H_{\text{eff}} = \Delta'_b b^\dagger b + \omega'_m m^\dagger m + \frac{G}{\sqrt{2}}(m^\dagger + m)(b^\dagger + b), \quad (21)$$

where $\Delta'_b \equiv \Delta_b - i\kappa_b$, $\omega'_m \equiv \omega_m - i\gamma_m$ and m (m^\dagger) is the annihilation (creation) operator for the mechanical mode, i.e., $x = (m + m^\dagger)/\sqrt{2}$, $p = (m - m^\dagger)/\sqrt{2}i$. Note this Hamiltonian is non-Hermitian due to the phenomenological dissipative factors and it shares a similar formation to the initial Hamiltonian in Ref. [46]. The mechanical mode and the probe mode in this effective Hamiltonian are coupled by a Rabi interaction, which is the sum of the Jaynes-Cummings (JC) interaction leading to the resonant splitting of modes and the counter-rotating terms that do not contribute to the stable dressed states. In the red-detuning situation $\Delta_b > 0$, one can find that the JC terms will survive by the long-time average via rotating the Hamiltonian in Eq. (21) to the interaction picture with respect to $\Delta_b b^\dagger b + \omega_m m^\dagger m$. While in the blue-detuning $\Delta_b < 0$, however, the counter-rotating terms become dominant.

A further explanation could be made about the normal frequencies, i.e., the eigenvalues of the Hamiltonian in Eq. (21). By the Bogoliubov transformation [47], they read

$$\begin{aligned} \omega_{\pm} &= \sqrt{\frac{\Delta'^2_b + \omega_m^2}{2} \pm \frac{1}{2}\sqrt{(\Delta'^2_b - \omega'^2_m)^2 + 8G^2\omega'_m\Delta'_b}} \\ &\approx \sqrt{\omega_m^2 \pm \sqrt{2G^2\Delta_b\omega_m}}, \end{aligned} \quad (22)$$

where the approximated solution in the second line is obtained with a large mechanical quality factor $\omega_m \gg \gamma_m$ and a resolved sideband $\omega_m \gg \kappa_b$. With the red-sideband $\Delta_b = \omega_m$, the frequency splitting $\Delta\omega \equiv \omega_+ - \omega_-$ is significant in the real part [see the normal-mode splitting in Fig. 2(a)(c)], unless $G/\omega_m > 1/\sqrt{2}$ inducing an unstable linear system due to Eq. (6). In addition, the splitting $\Delta\omega$ is proportional to the square root of the enhanced coupling strength \sqrt{G} . With the blue-sideband $\Delta_b = -\omega_m$, however, $\Delta\omega$ is dominated by an imaginary part and merely affects the modulus of the normal-mode frequencies. It thus gives rise to the avoided NMS in Fig. 2(b)(d).

Comparing Fig. 2(a)(c) and Fig. 2(b)(d), if one is interested to realize an appropriate metrology around the mechanical frequency, then one has to focus on the blue-sideband situation, in which the noise spectrum is nearly monotonic to the coupling strength. In the following section, it is further shown that the coherent quantum noise cancellation should also be performed within the blue-sideband condition.

IV. WEAK FORCE DETECTION WITH CQNC

Quantum detection or metrology under control targets on suppressing the measurement-induced noise so as to realize an ultrasensitive measurement beyond the standard quantum limit. As for the noise spectrum in Eq. (18), SQL in Eq. (20) is a compromise of the backaction noise weighted with $1/G^2$ and the shot noise weighted with G^2 . The CQNC technique could reduce the backaction noise [32, 33] so as to the overall noise. In this section, we apply the CQNC technique to our optomechanical cavity with two optical modes by coupling the probe mode with an ancillary mode. It is found that both the backaction noise and the background noise (independent on G) will be dramatically reduced.

The core idea of the CQNC proposal lies on the coupling between the probe mode- b and the ancillary mode- c . The extra noise induced by this coupling compensates the backaction noise on the mechanical oscillation with an opposite sign. The interaction between mode- b and mode- c can be divided into the JC terms realized by beam splitters (BS) and the counter-rotating terms realized by optical parametric amplifiers (OPA). Mode- c is tuned to be near-resonant with mode- b to avoid its interaction with mode- a . The Hamiltonian under the CQNC control can be obtained from the initial Hamiltonian in Eq. (1). In the rotating frame with respect to $H'_L = \omega_L(a^\dagger a + b^\dagger b + c^\dagger c)$, it reads

$$\begin{aligned} H' = & \Delta_a a^\dagger a + \Delta_b b^\dagger b + \Delta_c c^\dagger c + \frac{\omega_m}{2}(x^2 + p^2) \\ & + iE(a^\dagger - a) + gx(a^\dagger b + ab^\dagger) + g_1(bc^\dagger + b^\dagger c) \\ & + g_2(bc + b^\dagger c^\dagger), \end{aligned} \quad (23)$$

where c (c^\dagger) is the annihilation (creation) operator for the

ancillary mode and $\Delta_c \equiv \omega_c - \omega_L \approx \Delta_b$ is the detuning between the ancillary cavity and the driving laser. The last two terms in Eq. (23) are used for coherent cancellation. The JC terms weighted by g_1 describe a passive BS mixing the two cavity modes; while the counter-rotating terms weighted by g_2 are denoted by an active down-conversion dynamics of the two modes through a nondegenerate OPA. The strength of the JC interaction caused by BS is $g_1 = rc/L$, where r is the reflectivity, c is the speed of light, and L is the cavity length. The strength of the counter-rotating coupling is $g_2 = \Gamma lc/L$, where l is the crystal length and Γ is the gain parameter [33].

Now the full set of the Heisenberg-Langevin equations describing the dynamics of the total system reads,

$$\begin{aligned} \dot{a} &= -i\Delta_a a - igxb - \kappa_a a + \sqrt{2\kappa_a}a_{\text{in}} + E, \\ \dot{b} &= -i\Delta_b b - igxa - ig_1c - ig_2c^\dagger - \kappa_b b + \sqrt{2\kappa_b}b_{\text{in}}, \\ \dot{c} &= -i\Delta_c c - ig_1b - ig_2b^\dagger - \kappa_c c + \sqrt{2\kappa_c}c_{\text{in}}, \\ \dot{x} &= \omega_m p, \\ \dot{p} &= -\omega_m x - g(a^\dagger b + ab^\dagger) - \gamma_m p + F_{\text{in}}, \end{aligned} \quad (24)$$

where c_{in} is the vacuum noise operator for the ancillary mode satisfying $\langle c_{\text{in}}(t)c_{\text{in}}^\dagger(\tau) \rangle = \delta(t - \tau)$. Again, after the linearization procedure, the Heisenberg-Langevin equations for the fluctuation variables are

$$\begin{aligned} \dot{a} &= -i\Delta_a a - \kappa_a a + \sqrt{2\kappa_a}a_{\text{in}}, \\ \dot{b} &= -i\Delta_b b - iGx - i\frac{g_c}{2}c - i\frac{g_c}{2}c^\dagger - \kappa_b b + \sqrt{2\kappa_b}b_{\text{in}}, \\ \dot{c} &= -i\Delta_c c - i\frac{g_c}{2}b - i\frac{g_c}{2}b^\dagger - \kappa_c c + \sqrt{2\kappa_c}c_{\text{in}}, \\ \dot{x} &= \omega_m p, \\ \dot{p} &= -\omega_m x - G(b + b^\dagger) - \gamma_m p + F_{\text{in}}, \end{aligned} \quad (25)$$

where the coupling strengths $g_2 = g_1 \equiv g_c/2$ are chosen for a balanced configuration. Similar to Eq. (3), the dynamics of the driven mode- a is again decoupled from all the interested modes. It means that the measurement noise is immune to the fluctuations of the driven mode. The decoupling as well as the noise cancellation is ensured by the near-resonant condition $\Delta_c \approx \Delta_b$. From Eq. (25), one can write the equations of motion for the field quadratures of the mechanical oscillator and optical modes b and c :

$$\begin{aligned} \dot{x}_b &= \Delta_b p_b - \kappa_b x_b + \sqrt{2\kappa_b}x_{\text{in}}^b, \\ \dot{p}_b &= -\Delta_b x_b - \sqrt{2}Gx_b - g_c x_c - \kappa_b p_b + \sqrt{2\kappa_b}p_{\text{in}}^b, \\ \dot{x}_c &= \Delta_c p_c - \kappa_c x_c + \sqrt{2\kappa_c}x_{\text{in}}^c, \\ \dot{p}_c &= -\Delta_c x_c - g_c x_b - \kappa_c p_c + \sqrt{2\kappa_c}p_{\text{in}}^c, \\ \dot{x} &= \omega_m p, \\ \dot{p} &= -\omega_m x - \sqrt{2}Gx_b - \gamma_m p + F_{\text{in}}, \end{aligned} \quad (26)$$

where $x_c \equiv (c + c^\dagger)/\sqrt{2}$, $p_c \equiv (c - c^\dagger)/\sqrt{2}i$, $x_{\text{in}}^c \equiv (c_{\text{in}} + c_{\text{in}}^\dagger)/\sqrt{2}$, and $p_{\text{in}}^c \equiv (c_{\text{in}} - c_{\text{in}}^\dagger)/\sqrt{2}i$.

A flow chart about Eq. (26) is drafted in Fig. 3 to visualize how to build the antinoise coherent channel via

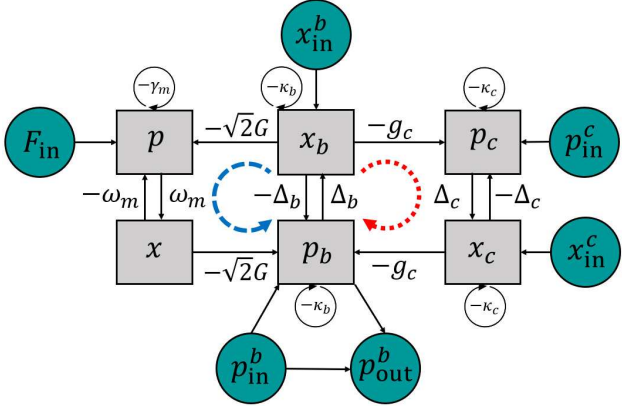


FIG. 3. (Color online) Flow chart for Eq. (26) and the input-output theory in Eq. (10). Arrows points from the variables on the right-hand side of Eq. (26) to the relevant variables on its left-hand side. The blue dashed curve describes the propagating path of the input noise x_{in}^b from the position quadrature x_b through the variables p and x to the probed phase quadrature p_b . The red dotted curve denotes the path provided by the ancillary mode having an opposite effect to compensate the blue one.

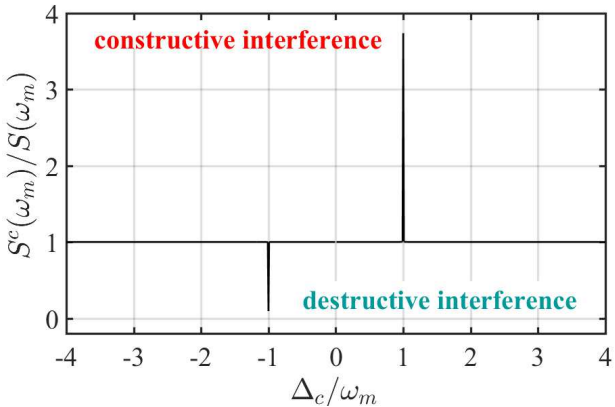


FIG. 4. (Color online) Ratio of the measurement noise spectrum under the CQNC protocol and that with no control by varying the ancilla-mode detuning. The measured frequency is set as the mechanical frequency $\omega = \omega_m$. The probe mode is set to be resonant with the ancillary mode $\Delta_b = \Delta_c$. The enhanced coupling strength between the probe mode and the mechanical oscillator is $G = 0.2\omega_m$ and the relaxation rate of the ancillary mode is $\kappa_c = 0.5\gamma_m$ as given in Eq. (30c). The other parameters are set the same as those in Fig. 2.

the ancillary mode. In the linear-response regime, the output field is the sum of the individual contributions from the input signals and noises. In our protocol for the weak-force metrology, the to-be-measured external force acting on the mechanical oscillator formally generates an input field (including signal and noise) to the probe mode, which propagates to the output signal through the quadrature variables p , x , and p_b in sequence due to Eq. (26). The backaction noise [32] x_{in}^b contributes to the output signal partially through the coupling between the

probe mode- b and the mechanical oscillator and partially through the coupling between the probe mode- b and the ancillary mode- c . The two processes are respectively distinguished by the blue dashed and the red dotted curves in Fig. 3. The ancillary coherent channel described by the red curve plays a central role in CQNC. It is verified that under the matching condition $\Delta_c = -\omega_m$, the ancillary mode behaves effectively as a mechanical oscillator with an negative frequency, equivalent to a mechanical oscillator with an effectively negative mass in Ref. [32]. Consequently the ancillary mode generates a backaction noise with an opposite sign to offset the one with no control, which facilitates a destructive quantum interference. In essence, with the assistance from the ancillary mode, the output noise spectrum for the probe mode in Eq. (18) is modified to

$$S^c(\omega) = S_{\text{th}} + \frac{g_c^2 \kappa_c |\chi_c(\kappa_c - i\omega)|^2}{2G^2 \Delta_c^2 |\chi_m|^2} + \frac{g_c^2 \kappa_c |\chi_c|^2}{2G^2 |\chi_m|^2} + \frac{1}{2} \left| \frac{\sqrt{\kappa_b} \chi_b \Delta_b - \sqrt{\kappa_b} \chi_b (g_c^2 \chi_c + 2G^2 \chi_m)}{G \chi_m} \right|^2 + \frac{1}{2} \left| \frac{1 - 2\kappa_b \chi_b + \Delta_b^2 \chi_b^2 - \Delta_b \chi_b^2 (g_c^2 \chi_c + 2G^2 \chi_m)}{2G \sqrt{\kappa_b} \chi_b \chi_m} \right|^2, \quad (27)$$

where the susceptibilities of the probe field, the mechanical oscillator and the ancillary field are respectively defined as

$$\chi_b \equiv \frac{1}{\kappa_b - i\omega}, \quad (28a)$$

$$\chi_m \equiv \frac{\omega_m}{\omega_m^2 - \omega^2 - i\omega\gamma_m}, \quad (28b)$$

$$\chi_c \equiv \frac{\Delta_c}{(\kappa_c - i\omega)^2 + \Delta_c^2}. \quad (28c)$$

An extra backaction noise $g_c^2 \chi_c$ emerges in the last two terms in Eq. (27), clearly showing its interference with the initial noise $2G^2 \chi_m$. Then an ideal noise cancellation by destructive interference requires

$$g_c^2 \chi_c + 2G^2 \chi_m = 0. \quad (29)$$

For simplicity, the coupling strength between the ancillary mode and the probe mode is set as

$$g_c^2 = 2G^2, \quad (30a)$$

which can be conveniently met by modulating BS and OPA. Consequently it is easy to find that $\chi_c = -\chi_m$. Then due to the definitions given in Eq. (28) and under the resolved sideband condition $\omega_m \gg \kappa_c$, it turns out that the ancilla-mode frequency should satisfy:

$$\Delta_c = -\omega_m, \quad (30b)$$

and meanwhile the linewidth of the mechanical oscillator is twice that of the ancillary mode

$$\gamma_m = 2\kappa_c. \quad (30c)$$

The effect from the quantum interference between the two coherent noisy channels (distinguished by the blue and red circles in Fig. 3) on the output noise spectrum is shown in Fig. 4 by the ratio $S^c(\omega_m)/S(\omega_m)$. Here we focus on the reduced noise spectrum around the mechanical-oscillator frequency ω_m by CQNC under the resonant condition $\Delta_b = \Delta_c$. One can observe two extremely sharp patterns about the destructive interference at the blue-sideband $\Delta_c = -\omega_m$ and the constructive interference at the red-sideband $\Delta_c = \omega_m$, respectively. This result justifies the conditions for CQNC presented in Eq. (30).

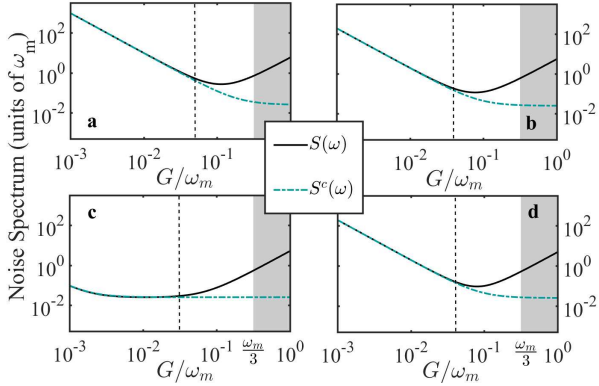


FIG. 5. (Color online) The measurement noise spectrums as functions of coupling-strength G with and with no control by CQNC. The frequencies of the probe mode and the ancillary mode are set as $\Delta_b = \Delta_c = -\omega_m$ in the blue-sideband situation. The measured frequencies are set as (a) $\omega = 0.94\omega_m$, (b) $\omega = 0.97\omega_m$, (c) $\omega = \omega_m$, and (d) $\omega = 1.03\omega_m$, respectively. The gray areas indicate the unstable regimes determined by the Routh-Hurwitz criterion, where the specified threshold value is found to be $G = \omega_m/3$ consistent with the other parameters as the same as those in Fig. 2.

The backaction noises in Eq. (27), i.e., the terms relevant to $g_c^2\chi_c + 2G^2\chi_m$, vanish under the ideal condition in Eq. (29). Then the noise spectrum with coherent cancellation reads,

$$S^c(\omega) = S_{\text{th}} + \kappa_c \frac{|\chi_c(\kappa_c - i\omega)|^2 + \Delta_c^2|\chi_m|^2}{\Delta_c^2|\chi_m|^2} + \frac{[(\Delta_b^2 - \omega^2 + \kappa_b^2)^2 + 4\kappa_b^2\omega^2](\omega^2\gamma_m^2 + \Delta^2)}{8G^2\kappa_b\omega_m^2(\omega^2 + \kappa_b^2)}. \quad (31)$$

In comparison to the noise spectrum without control $S(\omega)$ in Eq. (18), it is now found that the thermal and the shot noises are left invariant, the backaction noise is cancelled, and a new background noise induced by mode- c turns out to replace the old one proportional to the detuning Δ [the second term in Eq. (18)]. In Fig. 5, we show the numerical simulation of $S(\omega)$ (see the black-solid lines) and $S^c(\omega)$ (see the green-dot-dashed lines) at the working point $\Delta_b = \Delta_c = -\omega_m$ for CQNC by varying the coupling strength G between the probe mode and the mechanical mode.

It is shown that when increasing the coupling strength G , $S(\omega)$ for all the measured frequencies will firstly decrease and then rebound. The lower bound of $S(\omega)$, which is located at the optimized point $G = G_L$ determined by Eq. (19), is the standard quantum limit $S_L(\omega)$ given in Eq. (20). In the weak-coupling regime, the spectrum under CQNC $S^c(\omega)$ is almost the same as $S(\omega)$. When G is enhanced to approach the SQL point, $S^c(\omega)$ becomes significantly lower than $S(\omega)$ and will never rebound. For all the cases considered in Fig. 5, the control based on the destructive interference over the backaction noise begins to take effect for a moderate coupling strength ($10^{-2} < G/\omega_m < 10^{-1}$) and the minimum value of $S^c(\omega)$ will never be greater than the optimized $S(\omega)$. More precisely, the standard quantum limit is definitely broken through for all the near-resonant cases under control, as shown in Fig. 5(a)(b)(d). And performing the CQNC strategy in the resonant case [Fig. 5(c)] will give rise to $S^c(\omega) = S_L(\omega_m)$ when $G \geq G_L$, even though it does not continue to decrease as those for the off-resonant cases. In addition, an optimized coupling G_L is found to increase with the detuning between the measured frequency and the mechanical frequency ω_m . It renders that the control window (the working range for the measured frequency under CQNC) shrinks with the detuning magnitude, given the coupling strength is constrained by the system stability. As calculated in appendix A, the coupling strength should not be greater than about one third of the mechanical frequency $G < \omega_m/3$ with the parameters used in Fig. 2 to ensure that the total linear system is stable even under CQNC.

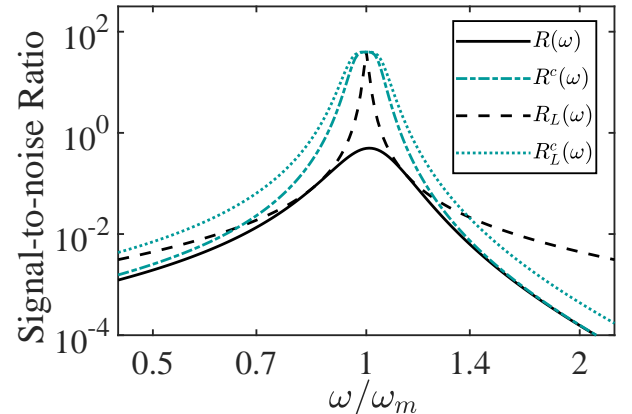


FIG. 6. (Color online) The signal-to-noise ratio as a function of the normalized frequency. The black-solid line and the green-dot-dashed line are respective the ratios with a fixed coupling strength $G = 0.2\omega_m$ in the absence and in the presence of control. The black-dashed line and the green-dotted line are the ratios with respective optimized coupling strengths in the absence and in the presence of control.

The high-sensitivity in quantum metrology can also be shown by the signal-to-noise ratio [44], which can be defined as $R(\omega) \equiv F_{\text{ext}}/S(\omega)$. Here the external force acting on the mechanical oscillator is assumed to be constant

for simplicity. In Fig. 6, we plot the SNRs obtained from the spectral density functions for four cases discussed in the preceding sections: (i) $S(\omega)$ in Eq. (18) with no control and with a fixed coupling strength $G = 0.2\omega_m$; (ii) $S^c(\omega)$ in Eq. (31) under the CQNC control and with $G = 0.2\omega_m$; (iii) $S_L(\omega)$ in Eq. (20) with no control yet with the optimized coupling strength G_L associated with SQL; and (iv) $S_L^c(\omega)$ evaluated also by Eq. (31) yet with the upper-bound coupling $G = \omega_m/3$ that respects the system stability. It is shown that the SNR at the mechanical-oscillator frequency ω_m can be improved by two orders in magnitude via either optimizing the coupling strength or performing the CQNC strategy. While the frequency range in which the SNR receives nearly the same amount of improvement under control is clearly much wider than that by coupling-strength optimization. Also it is found that to enhance the SNR as much as possible, one can apply the CQNC control in the low-frequency regime (in particular when $\omega < 1.4\omega_m$, see the green dotted line in Fig. 6) and use the G -optimization method in the high-frequency regime (see the black dashed line).

To understand the convergence of SNRs (R^c , R_L , and R_L^c) at $\omega = \omega_m$, one can compare the noise spectrums associated with them. Substituting Eqs. (30b) and (30c) into Eq. (31) and omitting the shot noise (scaling as G^{-2} and then being negligible for a large coupling strength), one can find that $S_L^c(\omega) \approx S_{th} + \kappa_c(\omega_m^2 + \omega^2 + \kappa_c^2)/\omega_m^2$. Regarding the resonant case $\omega = \omega_m$ and noting $\omega_m \gg \gamma_m, \kappa_c$, it converges to the SQL solution in Eq. (20): $S_L^c(\omega_m) \approx S_L(\omega_m) \approx S_{th} + 2\kappa_c$.

V. PHYSICAL REALIZATION

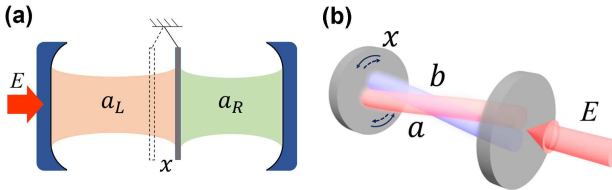


FIG. 7. (Color online). (a) Diagram of the mirror-in-the-middle optomechanical system consisting of a Fabry-Perot cavity with a high-reflectivity mirror mounted in the middle. The two optical modes a_L and a_R are coupled by the middle-mirror displacement. (b) Diagram of the torsional optomechanical system, in which an uniaxial medium is inserted. The cavity is weakly twisted with the torsional oscillation of the end mirror, which causes the mixing of the ordinary mode a , the extraordinary mode b and the mechanical mode x . The ordinary-mode frequency is larger than the extraordinary-mode frequency.

Now we consider the possible physical realizations of our protocol. The initial Hamiltonian in Eq. (1) could be realized by two types of optomechanical systems with two optical modes. A prototypical system consists of a Fabry-

Perot cavity with a high-reflectivity mirror mounted in the middle [37, 38] [see Fig. 7(a)]. The system Hamiltonian reads,

$$H = (\omega + fx)a_L^\dagger a_L + (\omega - fx)a_R^\dagger a_R - J(a_L^\dagger a_R + a_R^\dagger a_L), \quad (32)$$

where ω is the frequency of the two subcavities, f is the frequency shift per unit length and a_L (a_R) is the annihilation operator for the left (right) cavity mode and J indicates the coupling strength between the left and the right cavity modes. Note $f \approx -\omega/L$, where L is the cavity length in the high-reflectivity limit.

This Hamiltonian could be diagonalized by two normalized modes through the unitary transformation $a = (a_L + a_R)/\sqrt{2}$ and $b = (a_L - a_R)/\sqrt{2}$. Taking account the free energy of vibrating mirror and the external driving over mode- a into consideration, one can modify the Hamiltonian in Eq. (32) into

$$H' = \omega_a a^\dagger a + \omega_b b^\dagger b + \frac{\omega_m}{2}(x^2 + p^2) + g_m x(a^\dagger b + ab^\dagger) + iE(a^\dagger e^{-i\omega_L t} - ae^{i\omega_L t}), \quad (33)$$

where $\omega_{a,b} \equiv \omega \pm \sqrt{f^2 x^2 + J^2}$, $g_m = f$ and $|E| = \sqrt{P_{in}\kappa_a}/\omega_L$ is the driving strength.

Another experimental platform is a weakly twisted optomechanical cavity [41] with a birefringent medium inside [see Fig. 7(b)]. The two optical modes in this fire-new setup is the ordinary mode (marked as a) with a higher frequency ω_a and the extraordinary mode (marked as b) with a lower frequency ω_b . The torsional oscillation of the back mirror renders the mechanical mode coupled to the optical modes via permittivity tensor modulation. With the ordinary mode being driven by an external driving laser and the extraordinary mode being probed, the full Hamiltonian of the system can be written as

$$H = \omega_a a^\dagger a + \omega_b b^\dagger b + \frac{\omega_m}{2}(x^2 + p^2) + g_t x(a^\dagger b + ab^\dagger) + iE(a^\dagger e^{-i\omega_L t} - ae^{i\omega_L t}). \quad (34)$$

Here the coupling strength of the twisted optomechanical cavity is expressed by

$$g_t = -\frac{c}{16L\sqrt{n_e n_o}} \left(\frac{1}{n_o^2} - \frac{1}{n_e^2} \right), \quad (35)$$

where c is the light speed, L is the cavity length, and n_e and n_o are respectively the refractive indices of the extraordinary and the ordinary optical modes.

The noise spectral function for the weak-force measurement in SI unit of N^2/Hz could be obtained by rescaling the noise spectrum via $\tilde{\mathcal{S}}(\omega) \equiv \hbar m \omega_m \mathcal{S}(\omega)$ [33], where $\mathcal{S}(\omega)$ is selected from $S(\omega)$, $S^c(\omega)$, $S_L(\omega)$ or $S_L^c(\omega)$ in certain conditions. In Table I, we list the rescaled sensitivities for the four cases with various sensing frequencies, which are evaluated by typical parameters about an optomechanical system. In particular, the mechanical frequency $\omega_m = 2\pi \times 10.56\text{MHz}$, the mechanical-oscillator

TABLE I. Rescaled sensitivity of the optomechanical system to the weak force in the four cases discussed in Sec. IV with various sensing frequencies $\omega/\omega_m = 0.9, 1.0, 1.1$.

	$\tilde{\mathcal{S}}(\omega)^a$	$\tilde{\mathcal{S}}^c(\omega)^a$	$\tilde{\mathcal{S}}_L(\omega)^a$	$\tilde{\mathcal{S}}_L^c(\omega)^a$
$\omega/\omega_m = 0.9$	3.904	0.420	3.369	0.174
$\omega/\omega_m = 1$	1.515	0.035	0.035	0.035
$\omega/\omega_m = 1.1$	2.983	0.420	2.747	0.174

^a Units of $10^{-28} \text{ N}^2/\text{Hz}$.

mass $m = 48 \text{ pg}$ and the decay rate of the probe mode $\kappa_b = 2\pi \times 200 \text{ kHz}$ [3]. Regarding the linewidth of the ancillary cavity and the condition in Eq. (30c), a comparatively large damping rate (taken as $\gamma_m = 1.2 \times 10^{-3} \omega_m$ here) of the mechanical mode and a high- Q ancillary cavity are on demand. The former could be conveniently realized by setting the mechanical oscillator in ambient environments rather than in a low vacuum [48]. The latter is accessible in the low-loss ($\kappa/2\pi \sim 100 \text{ Hz}$) microwave cavities [49–51]. Comparing the second row of $\tilde{\mathcal{S}}^c(\omega)$ about the results under CQNC or the fourth row of $\tilde{\mathcal{S}}_L^c(\omega)$ about the results under both CQNC control and strong coupling to the first row of $\tilde{\mathcal{S}}(\omega)$ about those with no control, it is found that the sensitivities of the weak-force detection has been dramatically improved through our noise cancellation strategy. Particulary it is enhanced about two orders in magnitude at the near-resonant situation.

A twisted optomechanical system that consists of cantilever nanomechanical resonators integrated directly within an optical nanocavity is proposed to detect a torque with a sensitivity of $1.2 \times 10^{-20} \text{ Nm}/\sqrt{\text{Hz}}$ [48]. Using the typical parameters (the mechanical frequency $\omega_m = 2\pi \times 4.9 \text{ MHz}$, the oscillator mass $m = 427 \text{ fg}$, the mechanical quality factor $Q_m = \omega_m/\gamma_m = 21$ and the mirror length $r = 7.5 \mu\text{m}$), the improved sensitivity for weak-torque $\tilde{\mathcal{S}}_{\text{tor}}(\omega_m) \equiv r\sqrt{\hbar m\omega_m} \tilde{\mathcal{S}}_L^c(\omega_m)$ is found to be $7.75 \times 10^{-21} \text{ Nm}/\sqrt{\text{Hz}}$ under our CQNC strategy, also showing a better performance in torque detection.

VI. CONCLUSION

In this work, we have proposed a quantum metrology scheme about weak-force sensing in an optomechanical system consisting of two non-identical optical modes and a mechanical mode. The sensitivity for our weak-force metrology can be significantly enhanced to break though the standard quantum limit by using a coherent quantum noise cancellation strategy. In particular, our control strategy is performed by driving the high-frequency optical mode, probing the low-frequency optical mode and coupling the probe mode with a near-resonant ancillary mode. Under these deliberate and asymmetrical presumptions, one can build up an effective coherent noise channel to exactly eliminate the initial backaction noise,

and then remarkably reduce the entire noise-level to implement a high-precision metrology for the weak force on the mechanical mode.

Our proposal is accessible in both theory and experiment. The nanomechanical system is analysed in the standard linearization process by following the linear-response theorem. In the Heisenberg-Langevin equation and the effective Hamiltonian, the strong coupling between the optical modes and the mechanical mode is crucial to realize the high-precision metrology and also upper-bounded by the Routh-Hurwitz criterion for the linear-system stability. Two experimental platforms for the nanomechanical systems, the membrane-in-the-middle setup and the twisted-cavity-based weak-torque detector, are found to be possible implementations for our metrology protocol. With proper coupling strengths, we have shown dramatic improvements in terms of the rescaled sensitivity on the weak force or the weak torque.

ACKNOWLEDGMENTS

We acknowledge grant support from the National Science Foundation of China (Grants No. 11974311 and No. U1801661), Zhejiang Provincial Natural Science Foundation of China under Grant No. LD18A040001, and the Fundamental Research Funds for the Central Universities (No. 2018QNA3004).

Appendix A: The constraint on driving power by the linear-system stability

This appendix is about the Routh-Hurwitz criterion for constraining the pumping/driving power to ensure the linear-system stability.

We first consider the linearized Heisenberg-Langevin equation (3) for the free evolution of the system. The stability of the steady-state solution for the relevant linear differential equations can be determined by the eigenvalues of the associated Jacobian matrix. The solutions are stable if and only if the real part of every eigenvalue is negative. The differential equations in Eq. (3) decoupled from the driven mode are

$$\begin{aligned} \dot{b} &= -i\Delta_b b - ig\alpha x - \kappa_b b + \sqrt{2\kappa_b} b_{\text{in}}, \\ \dot{b}^\dagger &= i\Delta_b b^\dagger + ig\alpha^* x - \kappa_b b^\dagger + \sqrt{2\kappa_b} b_{\text{in}}^\dagger, \\ \dot{x} &= \omega_m p, \\ \dot{p} &= -\omega_m x - g(ab^\dagger + \alpha^* b) - \gamma_m p + F_{\text{in}}. \end{aligned} \quad (\text{A1})$$

It can be expressed in a compact form:

$$\dot{W} = A \cdot W + B, \quad (\text{A2})$$

where W and B are column vectors

$$W = [b, b^\dagger, x, p]^T, \quad B = [\sqrt{2\kappa_b} b_{\text{in}}, \sqrt{2\kappa_b} b_{\text{in}}^\dagger, 0, F_{\text{in}}]^T, \quad (\text{A3})$$

and A is a Jacobian matrix

$$A = \begin{pmatrix} -i\Delta_b - \kappa_b & 0 & -ig\alpha & 0 \\ 0 & i\Delta_b - \kappa_b & ig\alpha^* & 0 \\ 0 & 0 & 0 & \omega_m \\ -g\alpha^* & -g\alpha & -\omega_m & -\gamma_m \end{pmatrix}. \quad (\text{A4})$$

The characteristic function of A satisfies $a_0\lambda^4 + a_1\lambda^3 + a_2\lambda^2 + a_3\lambda + a_4 = 0$, where

$$\begin{aligned} a_0 &= 1, \\ a_1 &= \gamma_m + 2\kappa_b, \\ a_2 &= \Delta_b^2 + 2\gamma_m\kappa_b + \kappa_b^2 + \omega_m^2, \\ a_3 &= \gamma_m(\Delta_b^2 + \kappa_b^2) + 2\kappa_b\omega_m^2, \\ a_4 &= -2g^2|\alpha|^2\Delta_b\omega_m + \omega_m^2(\Delta_b^2 + \kappa_b^2). \end{aligned} \quad (\text{A5})$$

The Routh-Hurwitz stability criterion would constrain the system parameters through the Hurwitz determinants

$$\begin{aligned} D_1 &= a_1, \\ D_2 &= \begin{vmatrix} a_1 & a_3 \\ a_0 & a_2 \end{vmatrix}, \\ D_3 &= \begin{vmatrix} a_1 & a_3 & 0 \\ a_0 & a_2 & a_4 \\ 0 & a_1 & a_3 \end{vmatrix}, \\ D_4 &= \begin{vmatrix} a_1 & a_3 & 0 & 0 \\ a_0 & a_2 & a_4 & 0 \\ 0 & a_1 & a_3 & 0 \\ 0 & a_0 & a_2 & a_4 \end{vmatrix}. \end{aligned} \quad (\text{A6})$$

Note D_1 is positive. Thus according to the Routh-Hurwitz criterion, if and only if the following sequence of

the determinants of its principal submatrixs, i.e. $D_i (i = 2, 3, 4)$, are all positive, then the real part of the eigenvalues of A are all negative. A straightforward calculation shows that for $\Delta_b > 0$ (the red-detuning case),

$$|\alpha|^2 < \frac{(\Delta_b^2 + \kappa_b^2)\omega_m}{2|\Delta_b|g^2}, \quad (\text{A7})$$

and for $\Delta_b < 0$ (the blue-detuning case)

$$|\alpha|^2 > -\frac{(\Delta_b^2 + \kappa_b^2)\omega_m}{2|\Delta_b|g^2}. \quad (\text{A8})$$

Next we include the extra interaction between the probe mode and the ancilla mode, which will modify the previous constrain condition for the driving power measured by $|\alpha|$. The relevant differential equations due to Eq. (25) can be expressed by

$$\dot{W}_c = A_c \cdot W_c + B_c, \quad (\text{A9})$$

where

$$W_c = [b, b^\dagger, c, c^\dagger, x, p]^T, \quad (\text{A10a})$$

$$B_c = [\sqrt{2\kappa_b}b_{\text{in}}, \sqrt{2\kappa_b}b_{\text{in}}^\dagger, \sqrt{2\kappa_c}c_{\text{in}}, \sqrt{2\kappa_c}c_{\text{in}}^\dagger, 0, F_{\text{in}}]^T, \quad (\text{A10b})$$

$$A_c = \begin{pmatrix} -i\Delta_b - \kappa_b & 0 & -ig_1 & -ig_2 & -iG & 0 \\ 0 & i\Delta_b - \kappa_b & ig_2 & ig_1 & iG & 0 \\ -ig_1 & -ig_2 & -i\Delta_c - \kappa_c & 0 & 0 & 0 \\ ig_2 & ig_1 & 0 & i\Delta_c - \kappa_c & 0 & 0 \\ 0 & 0 & 0 & 0 & 0 & \omega_m \\ -G & -G & 0 & 0 & -\omega_m & -\gamma_m \end{pmatrix}. \quad (\text{A10c})$$

Then under the condition that $g_1 = g_2 = g_c/2$, the characteristic function for the Jacobian matrix A_c satisfies $a_0\lambda^6 + a_1\lambda^5 + a_2\lambda^4 + a_3\lambda^3 + a_4\lambda^2 + a_5\lambda + a_6 = 0$, where the coefficients are

$$\begin{aligned} a_0 &= 1, \\ a_1 &= \gamma_m + 2(\kappa_b + \kappa_c), \\ a_2 &= \omega_m^2 + \Delta_b^2 + \Delta_c^2 + 2(\gamma_m\kappa_c + \gamma_m\kappa_b + \kappa_c\kappa_b) + (\kappa_b + \kappa_c)^2, \\ a_3 &= \Delta_b^2(\gamma_m + 2\kappa_c) + \Delta_c^2(\gamma_m + 2\kappa_b) + 2\omega_m^2(\kappa_b + \kappa_c) + \gamma_m(\kappa_b + \kappa_c)^2 + 2\kappa_b\kappa_c(\gamma_m + \kappa_b + \kappa_c), \\ a_4 &= -\Delta_b(2G^2\omega_m + g_c^2\Delta_c) + \Delta_c^2\omega_m^2 + \Delta_b^2\omega_m^2 + \Delta_b^2\Delta_c^2 + \omega_m^2[(\kappa_b + \kappa_c)^2 + 2\kappa_b\kappa_c] + \Delta_b^2\kappa_c(2\gamma_m + \kappa_c) \\ &\quad + \Delta_c^2\kappa_b(2\gamma_m + \kappa_b) + \kappa_b\kappa_c(2\gamma_m\kappa_b + 2\gamma_m\kappa_c + \kappa_b\kappa_c), \\ a_5 &= -\Delta_b(4G^2\omega_m\kappa_c + g_c^2\Delta_c\gamma_m) + \gamma_m(\Delta_b^2 + \kappa_b^2)(\Delta_c^2 + \kappa_c^2) + 2\omega_m^2[\Delta_c^2\kappa_b + \Delta_b^2\kappa_c + \kappa_c\kappa_b(\kappa_b + \kappa_c)], \\ a_6 &= -\Delta_b\omega_m[g_c^2\Delta_c\omega_m + 2G^2(\Delta_c^2 + \kappa_c^2)] + \omega_m^2(\Delta_b^2 + \kappa_b^2)(\Delta_c^2 + \kappa_c^2). \end{aligned} \quad (\text{A11})$$

Now we have 6 Hurwitz determinants: D_i with i running from 1 to 6. The first 4 determinants share the same

formation as Eq. (A6). And the last 2 determinants read

$$D_5 = \begin{vmatrix} a_1 & a_3 & a_5 & 0 & 0 \\ a_0 & a_2 & a_4 & a_6 & 0 \\ 0 & a_1 & a_3 & a_5 & 0 \\ 0 & a_0 & a_2 & a_4 & a_6 \\ 0 & 0 & a_1 & a_3 & a_5 \end{vmatrix}, \quad D_6 = D_5 a_6 \quad (\text{A12})$$

Note again that D_1 is positive. Then all the other determinants should keep positive to met the Routh-Hurwitz criterion. With the parameters used in Fig. 2, one can have an approximate stable condition for the linear sys-

tem under control:

$$|\alpha|^2 \lesssim \frac{\omega_m^2}{9g^2}. \quad (\text{A13})$$

It indicated that for the system with CQNC, the enhanced coupling strength can not be greater than one third of the mechanical frequency $G \lesssim \omega_m/3$.

[1] M. Aspelmeyer, T. J. Kippenberg, and F. Marquardt, *Cavity optomechanics*, *Rev. Mod. Phys.* **86**, 1391 (2014).

[2] J. Chan, T. P. M. Alegre, A. H. Safavi-Naeini, J. T. Hill, A. Krause, S. Gröblacher, M. Aspelmeyer, and O. Painter, *Laser cooling of a nanomechanical oscillator into its quantum ground state*, *Nature* **478**, 89 (2011).

[3] J. D. Teufel, T. Donner, D. Li, J. W. Harlow, M. S. Allman, K. Cicak, A. J. Sirois, J. D. Whittaker, K. W. Lehnert, and R. W. Simmonds, *Sideband cooling of micromechanical motion to the quantum ground state*, *Nature* **475**, 359 (2011).

[4] A. Jöckel, A. Faber, T. Kampschulte, M. Korppi, M. T. Rakher, and P. Treutlein, *Sympathetic cooling of a membrane oscillator in a hybrid mechanical-atomic system*, *Nat. Nanotechnol.* **10**, 55 (2015).

[5] B. Abbott, R. Abbott, R. Adhikari, P. Ajith, B. Allen, G. Allen, R. Amin, S. B. Anderson, and W. G. Anderson, *Observation of a kilogram-scale oscillator near its quantum ground state*, *New J. Phys.* **11**, 073032 (2009).

[6] W.-Z. Zhang, J. Cheng, W.-D. Li, and L. Zhou, *Optomechanical cooling in the non-markovian regime*, *Phys. Rev. A* **93**, 063853 (2016).

[7] R. Ghobadi, S. Kumar, B. Pepper, D. Bouwmeester, A. I. Lvovsky, and C. Simon, *Optomechanical micro-macro entanglement*, *Phys. Rev. Lett.* **112**, 080503 (2014).

[8] W.-Z. Zhang, J. Cheng, J.-Y. Liu, and L. Zhou, *Controlling photon transport in the single-photon weak-coupling regime of cavity optomechanics*, *Phys. Rev. A* **91**, 063836 (2015).

[9] K. Zhang, F. Bariani, Y. Dong, W. Zhang, and P. Meystre, *Proposal for an optomechanical microwave sensor at the subphoton level*, *Phys. Rev. Lett.* **114**, 113601 (2015).

[10] A. Pontin, J. E. Lang, A. Chowdhury, P. Vezio, F. Marino, B. Morana, E. Serra, F. Marin, and T. S. Monteiro, *Imaging correlations in heterodyne spectra for quantum displacement sensing*, *Phys. Rev. Lett.* **120**, 020503 (2018).

[11] Y. Ma, S. L. Danilishin, C. Zhao, H. Miao, W. Z. Korth, Y. Chen, R. L. Ward, and D. G. Blair, *Narrowing the filter-cavity bandwidth in gravitational-wave detectors via optomechanical interaction*, *Phys. Rev. Lett.* **113**, 151102 (2014).

[12] J.-Q. Zhang, Y. Li, M. Feng, and Y. Xu, *Precision measurement of electrical charge with optomechanically induced transparency*, *Phys. Rev. A* **86**, 053806 (2012).

[13] C. L. Degen, F. Reinhard, and P. Cappellaro, *Quantum sensing*, *Rev. Mod. Phys.* **89**, 035002 (2017).

[14] V. Giovannetti, S. Lloyd, and L. Maccone, *Quantum metrology*, *Phys. Rev. Lett.* **96**, 010401 (2006).

[15] M. Aspelmeyer, T. J. Kippenberg, and F. Marquardt, *Cavity Optomechanics* (Springer Berlin Heidelberg, 2014).

[16] A. A. Clerk, M. H. Devoret, S. M. Girvin, F. Marquardt, and R. J. Schoelkopf, *Introduction to quantum noise, measurement, and amplification*, *Rev. Mod. Phys.* **82**, 1155 (2010).

[17] V. Peano, H. G. L. Schwefel, C. Marquardt, and F. Marquardt, *Intracavity squeezing can enhance quantum-limited optomechanical position detection through deamplification*, *Phys. Rev. Lett.* **115**, 243603 (2015).

[18] C. M. Caves, *Quantum-mechanical radiation-pressure fluctuations in an interferometer*, *Phys. Rev. Lett.* **45**, 75 (1980).

[19] A. Abramovici, W. E. Althouse, R. W. P. Drever, Y. Gürsel, S. Kawamura, F. J. Raab, D. Shoemaker, L. Sievers, R. E. Spero, K. S. Thorne, R. E. Vogt, R. Weiss, S. E. Whitcomb, and M. E. Zucker, *Ligo: The laser interferometer gravitational-wave observatory*, *Science* **256**, 325 (1992).

[20] T. P. Purdy, R. W. Peterson, and C. A. Regal, *Observation of radiation pressure shot noise on a macroscopic object*, *Science* **339**, 801 (2013).

[21] K. W. Murch, K. L. Moore, S. Gupta, and D. M. Stamper-Kurn, *Observation of quantum-measurement backaction with an ultracold atomic gas*, *Nat. Phys.* **4**, 561 (2008).

[22] R. S. Bondurant and J. H. Shapiro, *Squeezed states in phase-sensing interferometers*, *Phys. Rev. D* **30**, 2548 (1984).

[23] M. T. Jaekel and S. Reynaud, *Quantum limits in interferometric measurements*, *Europhys. Lett.* **13**, 301 (1990).

[24] A. Luis and L. L. Sánchez-Soto, *Multimode quantum analysis of an interferometer with moving mirrors*, *Phys. Rev. A* **45**, 8228 (1992).

[25] H. J. Kimble, Y. Levin, A. B. Matsko, K. S. Thorne, and S. P. Vyatchanin, *Conversion of conventional gravitational-wave interferometers into quantum nondestruction interferometers by modifying their input and/or output optics*, *Phys. Rev. D* **65**, 022002 (2001).

[26] S. Vyatchanin and E. Zubova, *Quantum variation measurement of a force*, *Physics Letters A* **201**, 269 (1995).

[27] F. Y. Khalili, *Optimal configurations of filter cavity in future gravitational-wave detectors*, *Phys. Rev. D* **81**, 122002 (2010).

[28] T. Briant, M. Cerdonio, L. Conti, A. Heidmann, A. Lobo, and M. Pinard, *Thermal and backaction noises in dual-sphere gravitational-wave detectors*, *Phys. Rev. D* **67**, 102005 (2003).

[29] T. Caniard, P. Verlot, T. Briant, P.-F. Cohadon, and A. Heidmann, *Observation of back-action noise cancel-*

lation in interferometric and weak force measurements, *Phys. Rev. Lett.* **99**, 110801 (2007).

[30] A. Buonanno and Y. Chen, *Quantum noise in second generation, signal-recycled laser interferometric gravitational-wave detectors*, *Phys. Rev. D* **64**, 042006 (2001).

[31] P. Verlot, A. Tavernarakis, T. Briant, P.-F. Cerdon, and A. Heidmann, *Backaction amplification and quantum limits in optomechanical measurements*, *Phys. Rev. Lett.* **104**, 133602 (2010).

[32] M. Tsang and C. M. Caves, *Coherent quantum noise cancellation for optomechanical sensors*, *Phys. Rev. Lett.* **105**, 123601 (2010).

[33] M. H. Wimmer, D. Steinmeyer, K. Hammerer, and M. Heurs, *Coherent cancellation of backaction noise in optomechanical force measurements*, *Phys. Rev. A* **89**, 053836 (2014).

[34] T. Wang, L. Wang, Y.-M. Liu, C.-H. Bai, D.-Y. Wang, H.-F. Wang, and S. Zhang, *Temperature-resistant generation of robust entanglement with blue-detuning driving and mechanical gain*, *Opt. Express* **27**, 29581 (2019).

[35] X.-W. Xu, L. N. Song, Q. Zheng, Z. H. Wang, and Y. Li, *Optomechanically induced nonreciprocity in a three-mode optomechanical system*, *Phys. Rev. A* **98**, 063845 (2018).

[36] B. Sarma and A. K. Sarma, *Unconventional photon blockade in three-mode optomechanics*, *Phys. Rev. A* **98**, 013826 (2018).

[37] X. Xu and J. M. Taylor, *Squeezing in a coupled two-mode optomechanical system for force sensing below the standard quantum limit*, *Phys. Rev. A* **90**, 043848 (2014).

[38] F. X. Sun, D. Mao, Y. T. Dai, Z. Ficek, Q. Y. He, and Q. H. Gong, *Phase control of entanglement and quantum steering in a three-mode optomechanical system*, *New J. Phys.* **19**, 123039 (2017).

[39] M. Bhattacharya and P. Meystre, *Multiple membrane cavity optomechanics*, *Phys. Rev. A* **78**, 041801 (2008).

[40] J. D. Thompson, B. M. Zwickl, A. M. Jayich, F. Marquardt, S. M. Girvin, and J. G. E. Harris, *Strong dispersive coupling of a high-finesse cavity to a micromechanical membrane*, *Nature* **452**, 72 (2008).

[41] D. Oue and M. Matsuo, *Twisting optomechanical cavity*, *arXiv:1912.06772*.

[42] E. X. DeJesus and C. Kaufman, *Routh-hurwitz criterion in the examination of eigenvalues of a system of nonlinear ordinary differential equations*, *Phys. Rev. A* **35**, 5288 (1987).

[43] S. Steinlechner, B. W. Barr, A. S. Bell, S. L. Danilishin, A. Gläfke, C. Gräf, J.-S. Hennig, E. A. Houston, S. H. Huttner, S. S. Leavey, D. Pascucci, B. Sorazu, A. Spencer, K. A. Strain, J. Wright, and S. Hild, *Local-oscillator noise coupling in balanced homodyne readout for advanced gravitational wave detectors*, *Phys. Rev. D* **92**, 072009 (2015).

[44] W.-Z. Zhang, L.-B. Chen, J. Cheng, and Y.-F. Jiang, *Quantum-correlation-enhanced weak-field detection in an optomechanical system*, *Phys. Rev. A* **99**, 063811 (2019).

[45] A. A. Clerk, F. Marquardt, and K. Jacobs, *Back-action evasion and squeezing of a mechanical resonator using a cavity detector*, *New J. Phys.* **10**, 095010 (2008).

[46] J. M. Dobrindt, I. Wilson-Rae, and T. J. Kippenberg, *Parametric normal-mode splitting in cavity optomechanics*, *Phys. Rev. Lett.* **101**, 263602 (2008).

[47] G. D. de Moraes Neto, F. M. Andrade, V. Montenegro, and S. Bose, *Quantum state transfer in optomechanical arrays*, *Phys. Rev. A* **93**, 062339 (2016).

[48] M. Wu, A. C. Hryciw, C. Healey, D. P. Lake, H. Jayakumar, M. R. Freeman, J. P. Davis, and P. E. Barclay, *Dissipative and dispersive optomechanics in a nanocavity torque sensor*, *Phys. Rev. X* **4**, 021052 (2014).

[49] A. Nunnenkamp, V. Sudhir, A. K. Feofanov, A. Roulet, and T. J. Kippenberg, *Quantum-limited amplification and parametric instability in the reversed dissipation regime of cavity optomechanics*, *Phys. Rev. Lett.* **113**, 023604 (2014).

[50] H. G. Leduc, B. Bumble, P. K. Day, B. H. Eom, J. Gao, S. Golwala, B. A. Mazin, S. McHugh, A. Merrill, D. C. Moore, O. Noroozian, A. D. Turner, and J. Zmuidzinas, *Titanium nitride films for ultrasensitive microresonator detectors*, *Appl. Phys. Lett.* **97**, 102509 (2010).

[51] M. R. Vissers, J. Gao, D. S. Wisbey, D. A. Hite, C. C. Tsuei, A. D. Corcoles, M. Steffen, and D. P. Pappas, *Low loss superconducting titanium nitride coplanar waveguide resonators*, *Appl. Phys. Lett.* **97**, 232509 (2010).